Colloids and Surfaces A 529 (2017) 959–965

Contents lists available at ScienceDirect

Colloids and Surfaces A

journal homepage: www.elsevier.com/locate/colsurfa

Research Paper

Bioinspired asymmetric-anisotropic (directional) fog harvesting based on the arid climate plant *Eremopyrum orientale*

M. Gürsoy[a], M.T. Harris[b], A. Carletto[b], A.E. Yaprak[c], M. Karaman[a,1], J.P.S. Badyal[b,1,*]

[a] Chemical Engineering Department, Selçuk University, Konya, 42075, Turkey
[b] Chemistry Department, Science Laboratories, Durham University, Durham DH1 3LE, England, UK
[c] Biology Department, Faculty of Science, Ankara University, Ankara 06100, Turkey

GRAPHICAL ABSTRACT

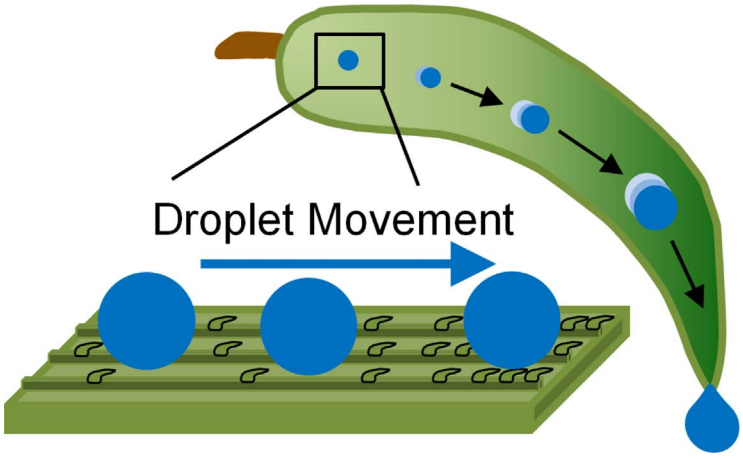

ARTICLE INFO

Keywords:
Fog harvesting
Water collection
Bioinspired
Hierarchical length-scales
Eremopyrum orientale
Functional nanoimprinting

ABSTRACT

Asymmetric-anisotropic (directional) fog collection behaviour is observed for leaves of the arid climate plant species *Eremopyrum orientale*. This is underpinned by a hierarchical surface structure comprising macroscale grooves, microscale tilted cones (in the direction of water flow), and nanoscale platelets. Soft lithography combined with either nanocoating deposition or functional nanoimprinting has been used to replicate this highly-efficient directional water collection mechanism.

1. Introduction

The asymmetric-directional flow of liquids along surfaces has a wide range of potential applications including microfluidics, lab-on-a-chip, sensors, microreactors, lubrication [1], inkjet printing [2], heat exchangers [3,4]. Asymmetric-anisotropic structures for such directional liquid flow have previously been observed in nature for shark skin denticles with ridges (riblets) which are understood to reduce drag

* Corresponding author.
E-mail address: j.p.badyal@durham.ac.uk (J.P.S. Badyal).
[1] These authors have made equal contributions.

http://dx.doi.org/10.1016/j.colsurfa.2017.06.065
Received 7 May 2017; Received in revised form 22 June 2017; Accepted 23 June 2017
Available online 24 June 2017

when aligned parallel to the direction of water flow [5], and butterfly wings, where nano-lamella are superimposed onto overlapping micro-scales causing water droplets to roll outwards radially [6]. In each of these cases, it is the oriented regular macro-scale structures which underpin the directional flow of water (with micro-scale grooves superimposed).

In this article, we describe the discovery of asymmetric-anisotropic fog collection behaviour for leaves of the *Eremopyrum orientale* plant species, which is found in arid climates such as North Africa, Southern Europe, South Western and Central Asia [7]. Such mechanisms for water harvesting from the air are important in relation to the development of cheap and environmentally-sustainable approaches for the supply of potable water for drinking and agricultural purposes in arid regions of the world [8–11]. Other reported fog collectors found in nature include spindle-knots of spider silk [12], barbed surfaces of *Hordeum vulgare* [13], cactus [14], twisted spiral desert geophytes [15], and fibrous hairs of the *Cotula fallax* and *Salsola crassa* plant species [16,17]. The gradient multi-length-scale surface structures of *Eremopyrum orientale* plant leaves have been successfully replicated in order to mimic the observed high efficiency asymmetric-anisotropic (directional) fog collection behaviour by either applying a hydrophobic nanocoating onto soft lithography replicas or using functional-nanoimprinting (which combines both physical replication and surface chemical functionalisation within the same soft lithography step [18]), Scheme 1.

2. Experimental

2.1. Plant species

Eremopyrum orientale plant leaves were obtained during the growing season (April) from near Lake Bolluk, located in Cihanbeyli-Konya, Turkey.

2.2. Replication

Plant leaves were rinsed with water to remove any surface debris and allowed to dry in air. Negative moulds of these surfaces were prepared by application of a polyvinylsiloxane base and cure mixture (President Plus Jet Light Body, Coltene/Whaledent AG) to the substrate [19,20], and immediately pressing down using a glass slide for a cure period of 10 min. Once the negative mould had hardened, it was carefully peeled away from the natural substrate surface, rinsed with water, and left to dry. Positive replicas from the negative moulds were prepared using epoxy resin (epoxy resin L and hardener S, R & G Faserverbundwerkstoffe GmbH). The epoxy resin was thoroughly mixed in a 5:2 ratio of resin to hardener, and then poured over the negative mould. Any trapped air bubbles were removed by placing under vacuum, and then the mixture was left to cure for 36 h in a desiccator. Finally, the negative moulds were gently peeled away to reveal the positive replica of the *Eremopyrum orientale* plant leaf.

Initiated chemical vapour deposition (iCVD) of hydrophobic surface nanocoatings was undertaken in a custom-built stainless steel chamber (20 cm width, 30 cm length, and 5 cm height) [21]. The chamber was connected to a two-stage rotary pump, with a butterfly-valve (MKS) located between the chamber and the pump, which was used to control the chamber pressure (monitored by a capacitance Baratron pressure transducer, MKS). This was achieved through a proportional–integral–derivative (PID) control unit (MKS), connected to both the pressure transducer and the butterfly-valve. Monomer 1H,1H,2H,2H-perfluorodecyl acrylate (PFDA, +97%, Sigma Aldrich) and initiator ditertbutyl peroxide (TBPO, +98%, Sigma Aldrich) were used as received, without further purification [22]. Each substrate sample was placed inside onto the base of the chamber (maintained at 35 °C using water cooling), followed by evacuation to system base pressure. Next, precursor and intitiator were vaporised inside stainless steel vessels connected to the chamber via needle control valves at predetermined pressures. A tungsten (+99.95%, 0.375 mm diameter, Alfa Aesar) filament array located 20 mm above the substrate surface was resistively heated using a variable transformer to initiate the polymerization reaction. Filament temperature during deposition was monitored using a K-type thermocouple (Omega) directly attached to one of the filaments. Depositions onto a reference silicon wafer were monitored by interferometry using a 632.8 nm He-Ne laser source. The deposition conditions used were as follows: 150 mtorr chamber pressure, 280 °C filament temperature, 0.5 sccm PFDA flowrate, 0.8 sccm TBPO flowrate. Upon completion of iCVD, the precursor feed valves were closed, and the chamber vented to atmosphere. 50 nm thickness nanocoatings were used.

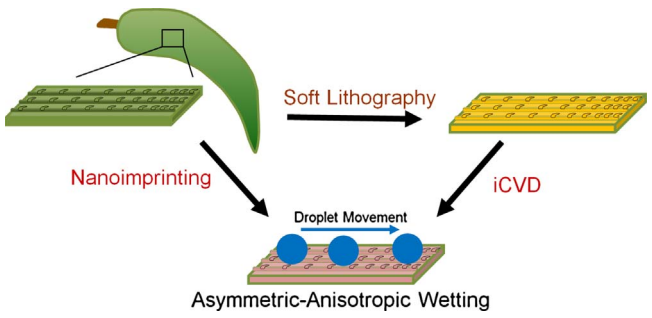

Scheme 1. Replication of Eremopyrum orientale plant leaf surface.

In the case of cure activated nanolayer transfer, a functional coating was plasma deposited onto the negative mould prior to the filling with epoxy resin to produce the positive replica. Pulsed plasma deposition of the low surface energy precursor, 1H, 1H, 2H, 2H-perfluorooctyl acrylate (+95%, Fluorochem Ltd, purified using several freeze-pump-thaw cycles) was carried out in an electrodeless cylindrical glass reactor (5 cm diameter, 520 cm^3 volume, base pressure of 1×10^{-3} mbar, and with a leak rate better than 1.8×10^{-9} kg s^{-1}) enclosed in a Faraday cage [23]. The chamber was fitted with a gas inlet, a Pirani pressure gauge, a 30 L min^{-1} two-stage rotary pump attached to a liquid cold trap, and an externally wound copper coil (4 mm diameter, 9 turns, spanning 8–15 cm from the precursor inlet). All joints were grease-free. An L-C network was used to match the output impedance of a 13.56 MHz radio frequency (RF) power generator to the partially ionised gas load. The RF power source was triggered by a signal generator, and the pulse shape monitored with an oscilloscope. Prior to each experiment, the chamber was cleaned by scrubbing with detergent, rinsing in water and propan-2-ol, followed by oven drying. The system was then reassembled and evacuated. Further cleaning consisted of running an air plasma at 0.2 mbar pressure and 50 W power for 30 min. Next, polyvinylsiloxane negative moulds, and reference silicon (100) wafer pieces (Silicon Valley Microelectronics Inc.) were inserted into the centre of the reactor, and the system pumped back down to base pressure. At this stage, 1H,1H,2H,2H-perfluorooctyl acrylate monomer vapour was introduced at a pressure of 0.2 mbar for 5 min prior to ignition of the pulsed electrical discharge. The optimum conditions for functional group retention corresponded to a peak power of 40 W, and a duty cycle on-time of 20 μs and off-time equal to 20 ms. Deposition was allowed to proceed for 150 s to yield 58 ± 5 nm thick layers [24]. Upon plasma extinction, the precursor vapour continued to pass through the system for a further 3 min, and then the chamber was evacuated back down to base pressure.

2.3. Characterisation

Photographs were taken using a camera (model Fujifilm FinePix S2950, Fujifilm Holdings, Japan). For higher magnification surface topography images, individual leaf specimens were prepared for scanning electron microscopy analysis by using a glycerol substitution process

[25]. These were fixed overnight using 25% gluteraldehyde (Sigma-Aldrich Co.) in phosphate buffer solution (pH 7.2, Sigma-Aldrich Co.). Next, 2–4 mL of 2% glutaraldehyde solution was dispensed onto a small (~2 cm^2) piece of fabric placed in a petri dish, and a leaf was placed on top of the soaked fabric for 2 h. The fabric was then replaced with a new piece, and it was soaked with a solution of 10% glycerol (> 99%, Sigma Aldrich Ltd.) and left for 2 h. The same process was repeated for increasing concentrations of glycerol up to 90% in 10% steps. No gold coating was used for the leaf samples due to the conductive nature of the glycerol [26]. Surface topography images were taken on a scanning electron microscope (Model LS-10 scanning electron microscope, Zeiss) operating in a secondary electron detection mode, in conjunction with 20 kV accelerating voltage, and a working distance between 9 and 11 mm. The epoxy resin positive replica samples were mounted onto a carbon disk supported on an aluminum holder, and coated with a 5 nm gold layer (Model 108 sputter coating unit, Cressington Scientific Instruments Ltd) in order to avoid excess surface charging. Images were taken on a scanning electron microscope (Cambridge Stereoscan 240) operating in secondary electron detection mode, in conjunction with 8 kV accelerating voltage, and a working distance between 8 and 26 mm. Surface features were analysed using image analysis software (ImageJ, public domain, http://rsbweb.nih.gov/ij/).

Microlitre sessile drop contact angle analysis was carried out with a video capture system (Model OCA 50, DataPhysics Instruments GmbH) using 2 μL dispensation of deionised water (BS 3978 grade 1). Advancing and receding contact angles were measured by respectively increasing and decreasing the droplet size until the contact line was observed to move [27]. A 9 μL water droplet size was employed for tilt angle measurements.

Mist collection measurements were undertaken by mounting each sample above an 11 mm inner neck diameter, 25 cm^3 volumetric flask (ISOLAB Laborgeräte GmbH), positioned on top of a mass balance, Supplementary Material Fig. S1. 0.5–6.0 μm mist droplets were generated using a 6 cm^3 chamber volume nebulizer (Freely Plus Model: V5002, Atılım Sağlık A.Ş.), with air flow rate of 10 L min^{-1} and 3.5 bar pressure delivering a water nebulisation rate of 0.4 cm^3 min^{-1}. These droplet sizes are comparable to meteorological fog [28]. The distance between sample front and nebulizer was set to 4 cm. All experiments were performed at 23 °C and repeated at least three times for each substrate sample type.

3. Results

3.1. Characterisation of plant

3.1.1. Optical microscopy

The *Eremopyrum orientale* plant grows to approximately 25 cm in height with leaves which are 5–8 cm long and approximately 1 cm wide, Fig. 1. The adaxial and abaxial surfaces are dark green and green respectively.

3.1.2. Contact angle

During fog episodes, water droplets coalesce and roll along the length of the leaf towards the underlying ground, Fig. 1 and Fig. 2. Of particular interest is that water droplets roll preferentially (asymmetric-anisotropic) along one direction towards the leaf tip (rather than the petiole). Both sides of the leaf display hydrophobicity, with the adaxial tip exhibiting the highest static water contact (164 ± 1°) and lowest hysteresis 5 ± 1° values (which is indicative of superhydrophobicity [29]) when viewed parallel (along) the length of each leaf, Table 1 and Fig. 3. A higher contact angle is measured when viewed parallel (along) versus perpendicular to the length of each leaf, which is consistent with anisotropic spreading along the leaf towards the tip. Measurement of the tilt angle for water droplets showed a preference to roll along the leaf towards the tip rather than perpendicular to the leaf axis, Supplementary Material Video S1 and Video S2.

3.1.3. Scanning electron microscopy

A hierarchical structure is visible on the adaxial leaf surface at higher magnifications, Fig. 4. There appears to be macro grooves running along the length of the leaf approximately 96 ± 13 μm apart, and their raised edges are covered with tilted cone-like structures (with a base diameter of 20 ± 7 μm) leaning away from the petiole towards the leaf tip (direction of rolling water droplet movement). The density of these tilted cone-like structures increasing on moving along the leaf towards the tip, which mirrors the rise in hydrophobicity, Fig. 5 and Fig. 3 respectively. On the nanoscale, the whole surface (excluding cones) is covered with 147 ± 31 nm width and 890 ± 169 nm length plant wax platelets.

3.2. Bioinspired replication

The *Eremopyrum orientale* plant leaf surface macro and micro scale physical structures were accurately replicated using soft lithography; however the nanoscale wax platelet definition was poor, which is consistent with the inherent limitation of this technique [18,19], and manifests in higher water contact angle hysteresis values, Fig. 4 and Table 1. These unfunctionalised positive replicas displayed anisotropic spreading of water droplets along the grooves, (resulting in an asymmetric shaped droplet) and enhanced directional mist collection, both of which follow the behaviour observed for the actual plant leaf surface, Table 1, Table 2, Fig. 3, and Fig. 6. Control experiments using flat polyethylene sheet and following iCVD perfluoroalkyl chain hydrophobic coating of flat polyethylene sheet showed no directional enhancement in water collection.

In order to achieve the high levels of hydrophobicity and low directional tilt angles observed for the *Eremopyrum orientale* leaf surface, the positive replicas were functionalised with perfluoroalkyl chains using either iCVD or functional nanoimprinting techniques. This helps to address the lower Cassie-Baxter hydrophobicity arising from the inherent limitation of poor nanoscale plant wax platelet definition associated with the soft lithography technique [18,19,30]. The obtained hydrophobic functionalised replica surfaces gave rise to asymmetric-anisotropic wetting enhancements far exceeding those associated with the unfunctionalised replica surface or the *Eremopyrum orientale* plant species, Fig. 6, Tables 1 and 2.

4. Discussion

Symmetric-anisotropic wetting of grooved plant leaf structures is known to give rise to either hydrophobicity or hydrophilicity depending upon the dimensional parameters employed [31–33]. The key factor for such water flow is understood to be the grooves running parallel to the long axis of the adaxial leaf surface, which guide the downslide of droplets once they have grown in size to the point at which the gravitational weight exceeds any droplet attachment mechanism. Simple grooved structures replicating such fog/water collection behaviour have previously been reported, although these do not provide enhanced forwards versus backwards (asymmetric) movement of water droplets along the grooves beyond 'downward with gravitational weight' effects [3,32,34–42]. Such symmetric anisotropic droplet spreading along grooves for fabricated model surfaces display higher contact angles when viewed along the grooves versus perpendicular [33,41,43–50], which is consistent with the present study, Table 1. Furthermore, the superimposition of micro-textures onto grooves to create hierarchical surfaces enhances anisotropic wetting akin to what is observed for the *Eremopyrum orientale* plant leaves, Fig. 4 [33,51–54].

For the case of asymmetric-anisotropic wetting of surfaces, previous model studies undertaken in the laboratory demonstrate such behaviours through the creation of either chemical gradient wettabilities [55] or equally-spaced tilted pillars prepared by reactive-ion-etching [56]. The accompanying theoretical model developed in the latter study, describes the criterion for directional liquid movement to be

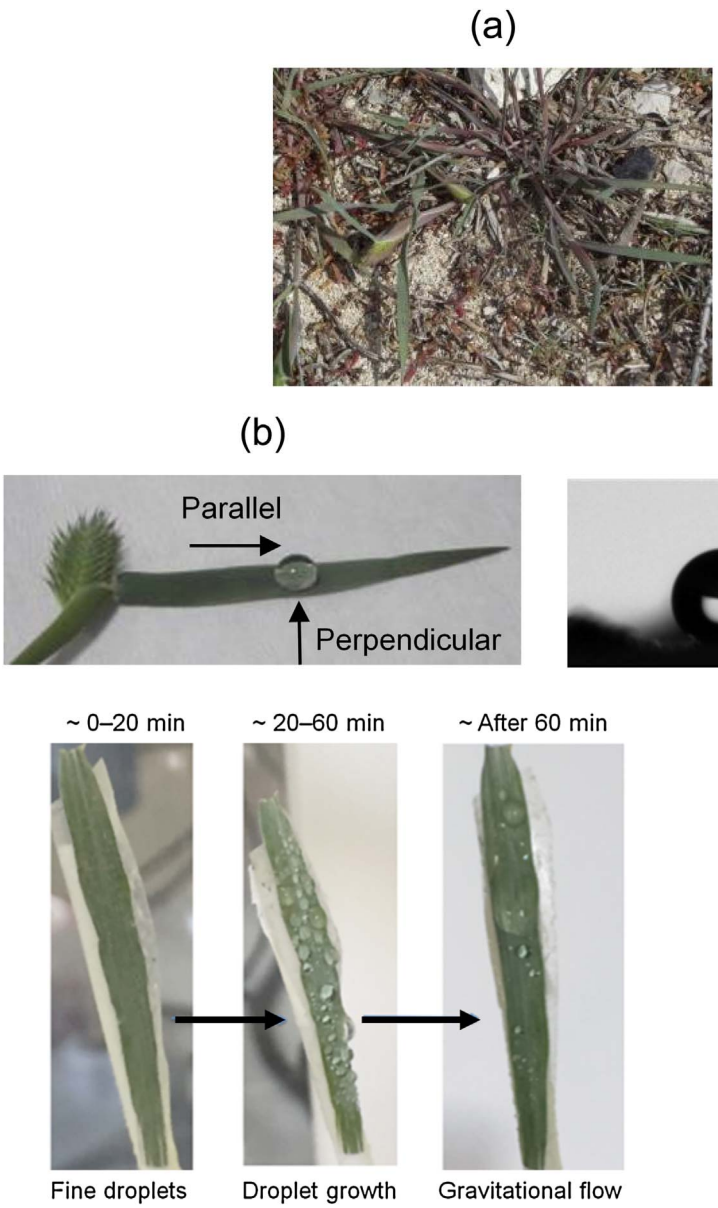

Fig. 1. Photographs of *Eremopyrum* orientale plant species taken in April during the growing season: (a) whole plant; (b) large water droplet placed on middle of adaxial surface; and (c) small water droplet placed near leaf tip of adaxial surface viewed along (parallel to) leaf axis from petiole towards tip (164 ± 1° static water contact angle).

Fig. 2. Mist collection on *Eremopyrum* orientale adaxial leaf surface over time (the white edges are paper used to support the leaf). Width of leaf is approximately 1 cm.

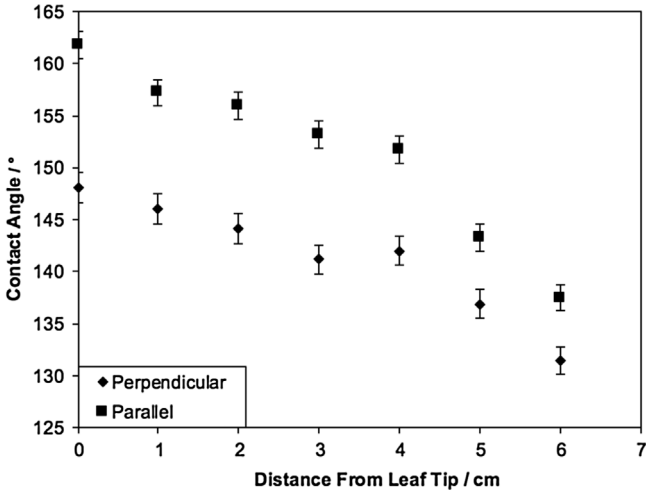

Fig. 3. Water contact angle values viewed parallel (along) and perpendicular to the length of *Eremopyrum* orientale plant adaxial leaf surface as a function of longitudinal distance from the leaf tip (total length 6 cm).

governed by the ability for droplet spreading to reach the next asymmetric surface protrusion [56]. In the present investigation, we have found that such asymmetric-anisotropic wetting is also present in nature on the adaxial surfaces of *Eremopyrum orientale* plant leaves, which is attributed to a hierarchical combination of grooves running along the length of the leaf (approximately 100 μm apart), and decreasing (non-regular) spaced tilted cones (approximate base diameter 20 μm) pointing towards the leaf tip (direction of water flow). The density of these tilted cone-like features increasing towards the leaf tip,

Table 1
Water contact angle and tilt angle water at which droplet starts to roll along *Eremopyrum* orientale adaxial leaf surface near leaf tip and positive replicas viewed parallel (along) and perpendicular to the length of each leaf. 2 μL and 9 μL water droplet sizes were employed for contact and tilt angle measurements respectively.

Sample	Contact Angle/°								Tilt Angle/°	
	Parallel				Perpendicular				Towards Tip	Towards Petiole
	Static	Advancing	Receding	Hysteresis	Static	Advancing	Receding	Hysteresis		
Leaf	164 ± 1	163 ± 1	157 ± 1	5 ± 1	148 ± 1	153 ± 1	145 ± 1	8 ± 1	22 ± 2	26 ± 2
Replica	132 ± 3	133 ± 2	94 ± 3	40 ± 4	70 ± 5	78 ± 4	35 ± 3	43 ± 4	Adhered[a]	Adhered[a]
iCVD replica	161 ± 2	162 ± 1	118 ± 5	43 ± 6	151 ± 1	153 ± 2	104 ± 4	49 ± 5	34 ± 2	38 ± 3
Functional nanoimprint replica	159 ± 3	161 ± 2	110 ± 3	52 ± 4	152 ± 3	154 ± 3	102 ± 3	53 ± 4	40 ± 4	43 ± 5

[a] The water droplet did not roll-off even when turned past 90°.

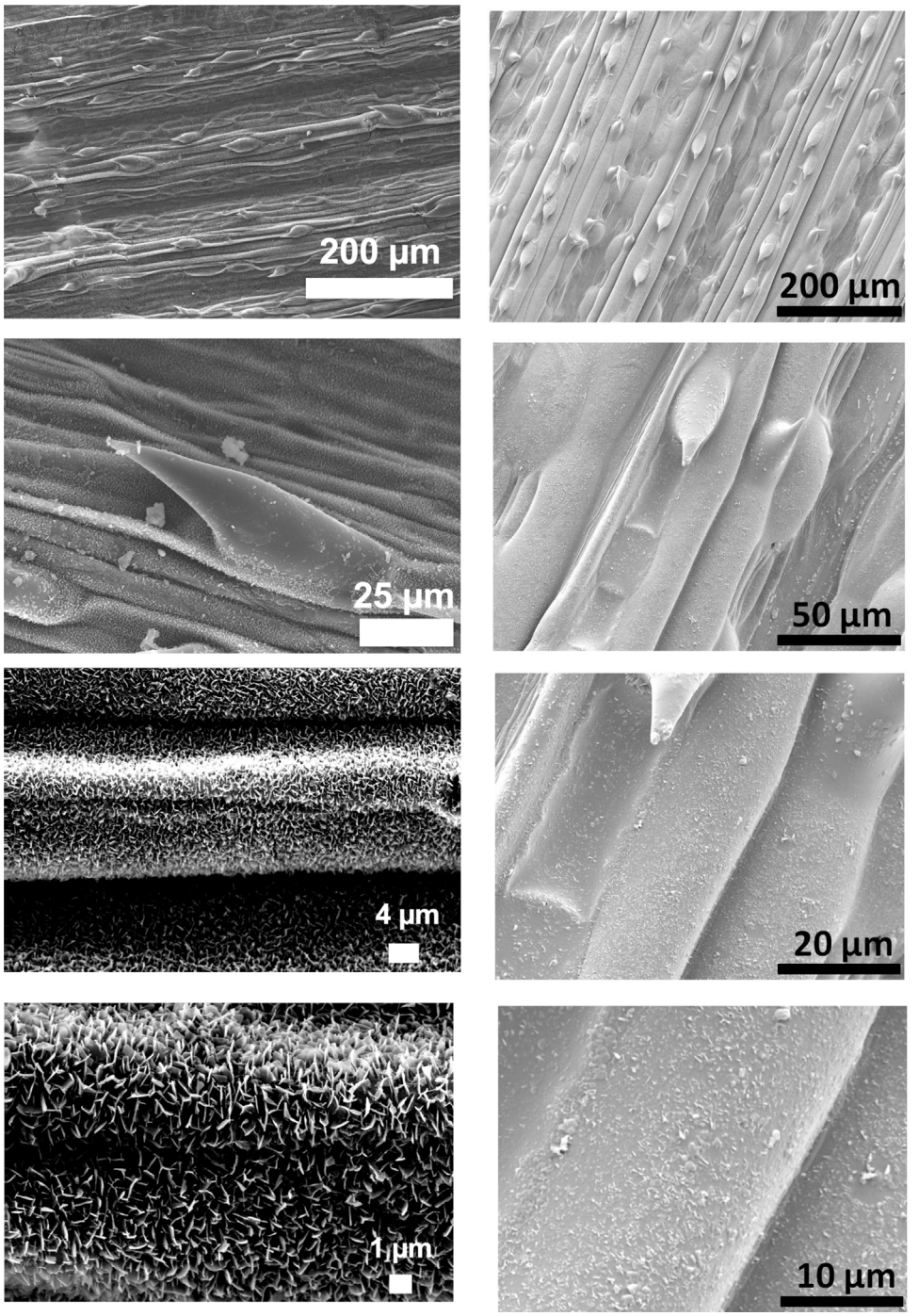

Fig. 4. SEM images of *Eremopyrum* orientale adaxial leaf middle region (left) and replica (right).

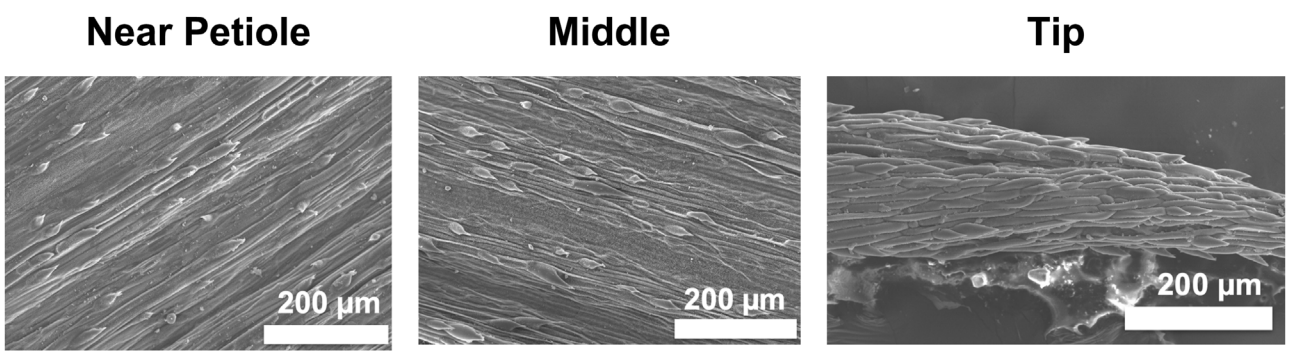

Fig. 5. SEM images taken along the length of *Eremopyrum* orientale adaxial leaf showing cones pointing towards tip (left to right).

Table 2
Mist collections efficiencies between 60 and 120 min for *Eremopyrum* orientale adaxial leaf and bioinspired functional surfaces, see Supplementary Material Fig. S2. Directional enhancement is defined as the increase in water collection efficiency for the leaf tip pointing downwards versus upwards.

Surface	Water Collection Efficiency/g $m^{-2} h^{-1}$		Directional
	Tip Pointing Upwards	Tip Pointing Downwards	Enhancement/%
Reference flat PE sample	58.8 ± 7.62	———	0
Reference iCVD functionalised flat polyethylene sample	80.8 ± 2.7	———	0
Leaf	104 ± 5.1	115.9 ± 2.2	11.6 ± 3.2
Unfunctionalised replica	90.8 ± 2.59	95.4 ± 1.0	5.1 ± 2.3
iCVD functionalised replica	106.9 ± 1.9	136.8 ± 7.8	27.9 ± 5.3
Functional nanoimprint replica	107.6 ± 3.15	129.2 ± 2.1	21.0 ± 4.4

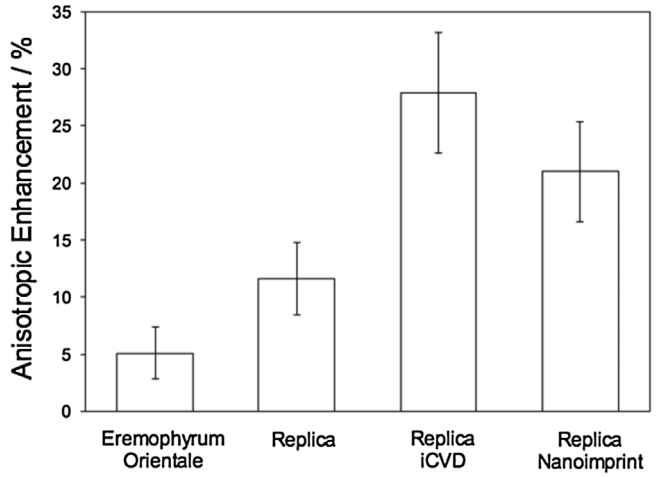

Fig. 6. Anisotropic (directional) enhancement of steady state mist collection efficiencies for micro-scale tilted cones pointing vertically downwards versus upwards for *Eremopyrum* orientale adaxial leaf, unfunctionalised replica, iCVD functionalised replica, and functional nanoimprint replica, see Supplementary Material Fig. S2.

which mirrors the rise in hydrophobicity attributable to the Cassie-Baxter effect [30], Fig. 5 and Fig. 3 respectively. In addition, the whole surface (excluding cones) is covered with nanoscale plant leaf wax platelets which also enhance hydrophobicity also due to Cassie-Baxter behaviour [30]. This should be contrasted with untilted regular spaced pyramidal (base 14 μm) hierarchical structures which do not display directional water collection [57] or anisotropic chemically patterned surfaces [58]. In terms of length scales, the physical structures present on *Eremopyrum orientale* plant leaf surfaces are reversed when compared to previously reported oriented (tilted) macro-scale surface structures containing superimposed micro-scale grooves for shark skin [5], butterfly wings [6], or plant leaves [59].

These *Eremopyrum orientale* plant leaf surface structures have been replicated by using either soft-lithography (which is a well-proven method for the physical replication of plant leaf structures [60–63]) or functional nanoimprinting (combines both physical replication and surface chemical functionalisation within the same soft lithography step [18]). The fabricated functionalised plant replica surfaces have shown enhanced levels of mist collection compared to corresponding flat surfaces which can be attributed to a combination of asymmetric-anisotropic wetting along the tilted cone containing grooved surfaces in association with hydrophobicity, Fig. 6. Asymmetric-anisotropic wetting along these hierarchical surfaces encourages directional movement of the collected water droplets, whilst hydrophobicity (to mimic nanoscale plant leaf wax platelets) lowers water droplet adhesion to the surface.

Given that around one billion people in the world lack access to clean drinking water (with many living in arid or semi-arid regions [64]) and three out of four jobs worldwide are water-dependent (stifling economic growth in developing countries [65]), such enhancements for water collection efficiencies are highly desirable. Other potential applications include microfluidics, lab-on-a-chip, sensors, microreactors, lubrication, inkjet printing, and heat exchangers.

5. Conclusions

Eremopyrum orientale plant leaf surfaces display asymmetric-anisotropic (directional) mist collection behaviour which is underpinned by a hierarchical surface structure comprising macro-scale grooves, micro-scale cones (tilted in the direction of water flow), and superimposed nanotexture. The density of tilted cones increases on moving from the leaf petiole to tip. These surfaces have been replicated by using soft lithography combined with either nanocoating deposition or functional nanoimprinting, and shown to be highly-efficient for directional mist collection.

Acknowledgements

This work was supported by Engineering and Physical Sciences Research Council (EPSRC) grant reference EP/J005401/1. M. Gürsoy was supported by The Scientific and Technological Research Council of Turkey (TÜBITAK) – BIDEB National Doctoral Fellowship Program. We thank R. Fraser for carrying out thickness measurements.

Appendix A. Supplementary data

Supplementary data associated with this article can be found, in the online version, at http://dx.doi.org/10.1016/j.colsurfa.2017.06.065.

References

[1] K. Hiratsuka, A. Bohno, H. Endo, Water droplet lubrication between hydrophilic and hydrophobic surfaces, J. Phys.: Conf. Ser. 89 (2007) 012012.
[2] J.Z. Wang, Z.H. Zheng, H.W. Li, W.T.S. Huck, H. Sirringhaus, Dewetting of conducting polymer inkjet droplets on patterned surface, Nat. Mater. 3 (2004) 171–176.
[3] A.D. Sommers, R. Yu, N.C. Okamoto, K. Upadhyayula, Condensate drainage performance of a plain fin-and-Tube heat exchanger constructed from anisotropic micro-grooved fins, Int. J. Refrig. 35 (2012) 1766–1778.
[4] D. Xia, L.M. Johnson, G.P. Lõpez, Anisotropic wetting surfaces with one-dimensional and directional structures: fabrication approaches, wetting properties and potential applications, Adv. Mater. 24 (2012) 1287–1302.
[5] D.W. Bechert, M. Bruse, W. Hage, Experiments with three-dimensional riblets as an idealized model of shark skin, Exp. Fluids 28 (2000) 403–412.
[6] Y. Zheng, X. Gao, L. Jiang, Directional adhesion of superhydrophobic butterfly wings, Soft Matter 3 (2007) 178–182.
[7] E. Cabi, M. Doğan, Taxonomic study on the genus *Eremopyrum* (Ledeb.) Jaub. et Spach (Poaceae) in Turkey, Plant Syst. Evol. 287 (2010) 129–140.
[8] W.J. Hamilton, M.K. Seely, Fog basking by the Namib desert beetle, *Onymacris unguicularis*, Nature 262 (1976) 284–285.
[9] O. Klemm, R.S. Schemenauer, A. Lummerich, P. Cereceda, V. Marzol, D. Corell, J. van Heerden, D. Reinhard, T. Gherezghiher, J. Olivier, P. Osses, J. Sarsour, E. Frost, M.J. Estrela, J.A. Valiente, G.M. Fessehaye, Fog as a fresh-water resource: overview and perspectives, Ambio 41 (2012) 221–234.
[10] O.M. Harb, M.Sh. Salem, G.H. Abd El-Hay, M. Makled Kh, Fog water harvesting providing stability for small Bedwe communities lives in north cost of Egypt, Ann. Agric. Sci. 61 (2016) 105–110.
[11] C. Potter, Measurements of fog water interception by shrubs on the California central coast, J. Coastal Conserv. 20 (2016) 315–325.
[12] H. Bai, J. Ju, R. Sun, Y. Chen, Y. Zheng, L. Jiang, Controlled fabrication and water collection ability of bioinspired artificial spider silks, Adv. Mater. 23 (2011) 3708–3711.
[13] M.A.K. Azad, W. Barthlott, K. Koch, Hierarchical surface architecture of plants as an inspiration for biomimetic fog collectors, Langmuir 31 (2015) 13172–13179.
[14] X. Heng, M. Xiang, Z. Lu, C. Luo, Branched ZnO wire structures for water collection inspired by cacti, ACS Appl. Mater. Interfaces 6 (2014) 8032–8041.
[15] S. Vogel, U. Müller-Doblies, Desert geophytes under dew and fog: the curly-whirlies of Namaqualand (South Africa), Flora 206 (2011) 3–31.

[16] H.G. Andrews, E.A. Eccles, W.C.E. Schofield, J.P.S. Badyal, Three-dimensional hierarchical structures for fog harvesting, Langmuir 27 (2011) 3798–3802.
[17] M. Gürsoy, M.T. Harris, J.O. Downing, S.N. Barrientos-Palomo, A. Carletto, A.E. Yaprak, M. Karaman, J.P.S. Badyal, Bioinspired fog capture and channel mechanism based on the arid climate plant Salsola crassa, Colloids Surf. A 529 (2017) 195–202.
[18] H.G. Andrews, T.J. Wood, W.C.E. Schofield, J.P.S. Badyal, Functional nanoimprinting, Chem. Vap. Deposition 18 (2012) 239–244.
[19] Y.N. Xia, E. Kim, X.M. Zhao, J.A. Rogers, M. Prentiss, G.M. Whitesides, Complex optical surfaces formed by replica molding against elastomeric masters, Science 273 (1996) 347–349.
[20] K. Koch, A.J. Sculte, A. Fischer, S.N. Gorb, W. Barthlott, A. Fast, Precise and low-cost replication technique for nano- and high-aspect-ratio structures of biological and artificial surfaces, Bioinspiration Biomimetics 3 (2008) 046002.
[21] M. Gürsoy, T. Uçar, Z. Tosun, M. Karaman, Initiation of 2-hydroxyethyl methacrylate polymerization by tert-butyl peroxide in a planar PECVD system, Plasma Processes Polym. 13 (2016) 438–446.
[22] M. Gupta, K.K. Gleason, Initiated chemical vapor deposition of poly(1H,1H,2H,2H-perfluorodecyl acrylate) thin films, Langmuir 22 (2006) 10047–10052.
[23] S.R. Coulson, I.S. Woodward, S.A. Brewer, C. Willis, J.P.S. Badyal, Ultra-Low surface energy plasma polymer films, Chem. Mater. 12 (2000) 2031–2038.
[24] R.C. Fraser, A. Carletto, M. Wilson, J.P.S. Badyal, Plasmachemical double click thiol–ene reactions for wet electrical barrier, ACS Appl. Mater. Interfaces 8 (2016) 21832–21838.
[25] H.J. Ensikat, W. Barthlott, Liquid substitution: a versatile procedure for SEM specimen preparation of biological materials without drying or coating, J. Microsc. 172 (1993) 195–203.
[26] H.J. Ensikat, Liquid substitution methods, in: A.W. Robards, A.J. Wilson (Eds.), Procedures in Electron Microscopy, John Wiley & Sons, York, UK, 1996, pp. 66–76.
[27] R.E. Johnson Jr., R.H. Dettre, Wettability, in: J.C. Berg (Ed.), Marcel Dekker, Inc., New York, 1993, pp. 1–75 (Chapter 1).
[28] J.A. Zak, Drop Size Distributions and Related Properties of Fog for Five Locations Measured From Aircraft. NASA Contractor Report 4585 DOT/FAA/CT-94/02, Langley Research Center, Virginia, USA, 2016, p. 1994. April.
[29] D. Öner, T.J. McCarthy, Ultrahydrophobic surfaces: effects of topography length scales on wettability, Langmuir 16 (2000) 7777–7782.
[30] A.B.D. Cassie, S. Baxter, Wettability of porous surfaces, Trans. Faraday Soc. 40 (1944) 546–551.
[31] L.F. Wang, Z.D. Dai, Effects of the natural microstructures on the wettability of leaf surfaces, Biosurf. Biotribol. 2 (2016) 70–74.
[32] A. Roth-Nebelsick, M. Ebner, T. Miranda, V. Gottschalk, D. Voigt, S. Gorb, T. Stegmaier, J. Sarsour, M. Linke, W. Konrad, Leaf surface structures enable the endemic Namib desert grass Stipagrostis sabulicola to irrigate itself with fog water, J. R. Soc. Interface 9 (2012) 1965–1974.
[33] S.G. Lee, H.S. Lim, D.Y. Lee, D. Kwak, K. Cho, Tunable anisotropic wettability of rice leaf-like wavy surfaces, Adv. Funct. Mater. 23 (2013) 547–553.
[34] S. Herminghaus, M. Brinkmann, R. Seemann, Wetting and dewetting of complex surface geometries, Annu. Rev. Mater. Res. 38 (2008) 101–121.
[35] Z. Yoshimitsu, A. Nakajima, T. Watanabe, K. Hashimoto, Effects of surface structure on the hydrophobicity and sliding behavior of water droplets, Langmuir 18 (2002) 5818–5822.
[36] X. Gao, X. Yao, L. Jiang, Effects of rugged nanoprotrusions on the surface hydrophobicity and water adhesion of anisotropic micropatterns, Langmuir 23 (2007) 4886–4891.
[37] P. Li, J. Xie, Z. Deng, Characterization of irregularly micro-structured surfaces related to their wetting properties, Appl. Surf. Sci. 335 (2015) 29–38.
[38] X. Yang, X. Liu, Y. Lu, J. Song, S. Huang, S. Zhou, Z. Jin, W. Xu, Controllable water adhesion and anisotropic sliding on patterned superhydrophobic surface for droplet manipulation, J. Phys. Chem. C 120 (2016) 7233–7240.
[39] D. Wu, J.N. Wang, S.Z. Wu, Q.D. Chen, S. Zhao, H. Zhang, H.B. Sun, L. Jiang, Three-level biomimetic rice-leaf surfaces with controllable anisotropic sliding, Adv. Funct. Mater. 21 (2011) 2927–2932.
[40] R.D. Narhe, D.A. Beysens, Nucleation and growth on a superhydrophobic grooved surface, Phys. Rev. Lett. 93 (2004) 076103.
[41] D. Wu, Q.D. Chen, J. Yao, Y.C. Guan, J.N. Wang, L.G. Niu, H.H. Fang, H.B. Sun, A simple strategy to realize biomimetic surfaces with controlled anisotropic wetting, Appl. Phys. Lett 96 (2010) 053704.
[42] N.J. Shirtcliffe, G. McHale, M.I. Newton, Learning from superhydrophobic plants: the use of hydrophilic areas on superhydrophobic surfaces for droplet control, Langmuir 25 (2009) 14121–14128.
[43] R. Kannan, D. Sivakumar, Drop impact process on a hydrophobic grooved surface, Colloids Surf. A 317 (2008) 694–704.
[44] D. Xia, L.M. Johnson, G.P. Lopez, Anisotropic wetting surfaces with one-dimensional and directional structures: fabrication approaches, wetting properties and potential applications, Adv. Mater. 24 (2012) 1287–1302.
[45] T.-I. Kim, K.Y. Suh, Unidirectional wetting and spreading on stooped polymer nanohairs, Soft Matter 5 (2009) 4131–4135.
[46] P. Li, J. Xie, J. Cheng, K.K. Wu, Anisotropic wetting properties on a precision-ground micro-V-grooved Si surface related to their micro-characterized variable, J. Micromech. Microeng 24 (2014) 075004.
[47] S. Zhao, H. Xia, D. Wu, C. Lv, Q.-D. Chen, K. Ariga, L.-Q. Liu, H.-B. Sun, Mechanical stretch for tunable wetting from topological PDMS film, Soft Matter 9 (2013) 4236–4240.
[48] S.Z. Wu, D. Wu, J. Yao, Q.D. Chen, J.N. Wang, L.G. Niu, H.H. Fang, H.B. Sun, One-step preparation of regular micropearl arrays for two-direction controllable anisotropic wetting, Langmuir 26 (2010) 12012–12016.
[49] Y. Lu, L. Yu, Z. Zhang, S. Wu, G. Li, P. Wu, Y. Hu, J. Li, J. Chu, D. Wu, Biomimetic surfaces with anisotropic sliding wetting by energy-modulation femtosecond laser irradiation for enhanced water collection, RSC Adv. 7 (2017) 11170–11179.
[50] C. Ma, S. Bai, X. Peng, Y. Meng, Anisotropic wettability of laser micro-grooved SiC surfaces, Appl. Surf. Sci. 284 (2013) 930–935.
[51] Y. Wan, Z. Lian, J. Xu, Z. Weng, X. Yin, H. Yu, Fabrication of the stainless steel surface with super durable one-direction superhydrophobicity and two-direction anisotropic wettability, Micro Nano Lett. 9 (2014) 712–716.
[52] D. Xia, S.R.J. Brueck, Strongly anisotropic wetting on one-dimensional nanopatterned surfaces, Nano Lett. 8 (2008) 2819–2824.
[53] P. Guo, Y. Lu, K.F. Ehmann, J. Cao, Generation of hierarchical micro-structures for anisotropic wetting by elliptical vibration cutting, CIRP Ann. 63 (2014) 553–556.
[54] X. Yang, J. Song, W. Xu, X. Liu, Y. Lu, Y. Wang, Anisotropic sliding of multiple-level biomimetic rice-leaf surfaces on aluminium substrates, Micro Nano Lett. 8 (2013) 801–804.
[55] S. Feng, S. Wang, L. Gao, G. Li, Y. Hou, Y. Zheng, Controlled directional water-droplet spreading on a high-adhesion surface, Angew. Chem. Int. Ed. 53 (2014) 6163–6167.
[56] K.-H. Chu, R. Xiao, E.N. Wang, Uni-directional liquid spreading on asymmetric nanostructured surfaces, Nat. Mater. 9 (2010) 413–417.
[57] X. Chen, J. Wu, R. Ma, M. Hua, N. Koratkar, S. Yao, Z. Wang, Nanograssed micropyramidal architectures for continuous dropwise condensation, Adv. Funct. Mater. 21 (2011) 4617–4623.
[58] K.K. Varanasi, M. Hsu, N. Bhate, W. Yang, T. Deng, Spatial control in the heterogeneous nucleation of water, Appl. Phys. Lett. 95 (2009) 094101.
[59] H. Chen, P. Zhang, L. Zhang, H. Liu, Y. Jiang, D. Zhang, Z. Han, L. Jiang, Continuous directional water transport on the peristome surface of Nepenthes alata, Nature 532 (2016) 85–89.
[60] Y.Y. Yan, N. Gao, W. Barthlott, Mimicking natural superhydrophobic surfaces and grasping the wetting process: a review on recent progress in preparing superhydrophobic surfaces, Adv. Colloid Interface Sci. 169 (2011) 80–105.
[61] E. Celia, T. Darmanin, E. Taffin de Givenchy, S. Amigoni, F. Guittard, Recent advances in designing superhydrophobic surfaces, J. Colloid Interface Sci. 402 (2013) 1–18.
[62] A.T. Abdulhussein, G.K. Kannarpady, A.B. Wright, A. Ghosh, A.S. Biris, Current trend in fabrication of complex morphologically tunable superhydrophobic nano scale surfaces, Appl. Surf. Sci. 384 (2016) 311–332.
[63] M. Sun, C. Luo, L. Xu, H. Ji, Q. Ouyang, D. Yu, Y. Chen, Artificial lotus leaf by nanocasting, Langmuir 21 (2005) 8978–8981.
[64] The United Nations World Water Development Report, Managing Water Under Uncertainty and Risk, UNESCO, Paris, 2012.
[65] The United Nations World Water Development Report, Water and Jobs, UNESCO, Paris, 2016.